# Reliability of strain monitoring of composite structures via the use of optical fibre ribbon tapes for structural health monitoring purposes

T.H. Loutas[1,], P. Charlaftis[1], A. Airoldi[2], P.Bettini[2], C. Koimtzoglou[3], V. Kostopoulos[1*]

[1] Applied Mechanics Laboratory, Mechanical Engineering & Aeronautics Department, University of Patras

[2]Dept. of Aerospace Science and Technology, Politecnico di Milano, Italy

[3]INASCO Hellas Co; Athens, Greece

* Corresponding author, e-mail address: kostopoulos@mech.upatras.gr

## Abstract

In aerospace industry, a lot of effort has been focused on the practical implementation of optical fibres on composite subcomponents for health monitoring purposes during the service life of an aircraft. To this direction the fibre optic ribbon tapes (FORTs) concept was developed in order to ease the handling, the surface placement and the maintenance of such sensitive sensors. In this paper, we investigate the structural durability of this concept comparing two ways of mounting the FORT (co-bonding and secondary bonding) under fatigue loading conditions. Through long term fatigue tests and utilizing additional experimental (electrical strain gauges (ESG)), theoretical as well as numerical tools, it is concluded that the deviation of the experimentally measured strains using the FORT approach versus conventional ESG values are well within an error of maximum 6%. Moreover, they remain in this error bound for as much as $10^6$ loading cycles, rendering FORTs a reliable solution for aerospace SHM. In the final part of the study, the effect of the FORTs placement on the stiffness of a structure is assessed through numerical analysis of the changes of the dynamic characteristics as well as the modal response of an aeronautical subcomponent representative of a wing front spar.

Keywords: Structural Health Monitoring (SHM), Fiber Bragg Gratings, reliability of measurements, metrology

## 1. Introduction

The continuously growing composites industry combined with the global effort to reduce maintenance costs across industrial applications and also the need for better utilization of resources and materials create the ground for novel structural health monitoring systems (SHM) to be developed. The need for reliable use of high performance composite materials to aerospace structures is a characteristic example [1], hence the implementation of health monitoring techniques that enhance the safe operation of a structure is of top priority. Researchers across the world are working to this direction. Examples of lab-scale and relatively low to medium Technology Readiness Level (TRL) systems with the ability to monitor physical and/or mechanical properties (i.e. temperature, strain, displacement, acceleration) of structures during pre-defined operating conditions are abundant in the relevant literature [1-5].

From the variety of SHM techniques, a lot of attention has been devoted the last 20 years on strain sensing with optical fibers with inscribed FBG sensors. FBGs are a state-of-the-art class of sensors that have been recognized to suit this purpose for various structural applications [6-8]. They are used for sensing applications, for measuring temperature, strain, pressure, refractive index etc. They offer many advantages over classic electrical sensing devices. Among the most important ones is their advantage of multiplexing by using different wavelength of light for each sensor. Hence, a large number of optical sensors can be inscribed in a single fibre optic cable utilizing only one channel in the interrogation unit. Worth

mentioning in the case of composite structures, is their flexibility to be placed either on the surface of the composite component of interest, or embedded inside the composite structure [9]. The integration of optical fiber sensors into the composite material could allow potentially in situ curing monitoring during the manufacturing process, and further on, the same sensors can be utilized for the component qualification/approval, as well as for the monitoring of the structural integrity during its service life [10]. The concept of embedment, despite its advantages, is under certain criticism since it is argued that the mechanical properties of the host structure degrade [11], since the region of material around the embedded FBG is a potential site of damage initiation and additionally the maintainability of the sensor network in case of sensor/optical fibre failure becomes questionable. Other studies [12–15] support that the influence of the optical fiber is negligible if deployed in the direction of the reinforcement fibers. No decreased properties have been reported on specimens with optical fibers when subjected to tensile, bending or even inter-laminar shear stress tests. Especially for the aeronautics industry, an otherwise certified-to-fly material with an embedded sensor network is regarded as a new material that requires the long and costly process of full certification.

A number of studies have focused on their metrological characteristics trying to assess their performance as compared to the "conventional" electrical strain gauges (ESGs). In [16], Baere et al. study the reliability of FBG sensors embedded and surface attached in thermoplastic composites for half a million cycles. The FBG readings from the embedded sensor are compared with the extensometer measurements showing excellent correlation of the measured strains despite the fact that the two measuring devices actually measure strain at different locations. Excellent operation of the FBG sensor is reported throughout the whole duration of the fatigue test. In an earlier study in [17] De Waele et al. conducted a similar study during quasi-static loading of composite pressure vessels with main focus on assessing the reliability

and accuracy of FBG versus ESG sensors. They conclude on the clear superiority and stability of FBG sensors reporting a difference of 5-10% with the measurements acquired via ESGs. Groves et al. [18] compare surface strain measurements from a hydrostatically loaded ABS pipe with three techniques: speckle shearography, FBG sensors and ESG sensors to find reasonable agreement between experimental and theoretically calculated axial and hoop strains. They report variations of FBG versus ESG values of maximum 10% for axial strains and only 0.1% for hoop strains attributing high variations to slight misalignment of the respective sensors as well as local inhomogeneities (defects, non-uniform thickness) of the structure. FBG values from theoretically obtained ones deviate as much as 4% and 7%.

Friebele et al [19, 20] performed cyclic tests (100 cycles) on a composite C-channel instrumented with an array of FBG sensors to assess the survivability and reliability of the embedded sensors. Good agreement with surface bonded strain gauges was observed. Kalamkarov et al [21] conducted a wide range of experimental tests focusing on the long-term performance of FBG sensors embedded in composite materials. Specimens with embedded FBG sensors were subjected to multiple loading cycles and it was shown that the sensor output offered excellent agreement with the results of a surface mounted extensometer. In addition, dynamic tests were conducted in which the FBG sensors were subjected to trapezoidal and sinusoidal waveform loadings. The authors reported that the strain output of the sensors again agreed very well with that of the extensometer. In another study, Mrad et al [22] conducted cyclic load tests to evaluate the reliability, durability, and fatigue life performance of bonded FBG sensors. It was shown that bonded FBGs exhibit longer fatigue lives than electrical strain gauges.

The present work aims to prove the reliability of the concept of a fibre optic ribbon tape (FORT) to provide accurate and repeatable strain measurements under prolonged cyclic loading of one million cycles at high strain levels (up to 4000 με). FORTs are actually pre-

cured ribbon tapes that are separately produced by embedding the optical fiber(s) between two compliant laminas of glass/epoxy woven fabric prepreg. This concept eases the handling, mounting and replacement of the optical fibers on a structure and protects them during service conditions. Two different technological approaches were examined regarding the mounting of the FORT on a composite structure i.e. via secondary adhesive bonding or via co-bonding during the manufacturing autoclave process. A direct comparison of the experimentally acquired measurements with the FORT versus experimental measurements from ESGs as well as theoretical and numerical ones is realized, providing with interesting correlations and conclusions on the whole strain sensing approach. Additionally, the effect of the FORTs placement on the stiffness of a structure is assessed through an analysis of the changes in the dynamic characteristics and the modal response of an aeronautical subcomponent representative of a wing front spar.

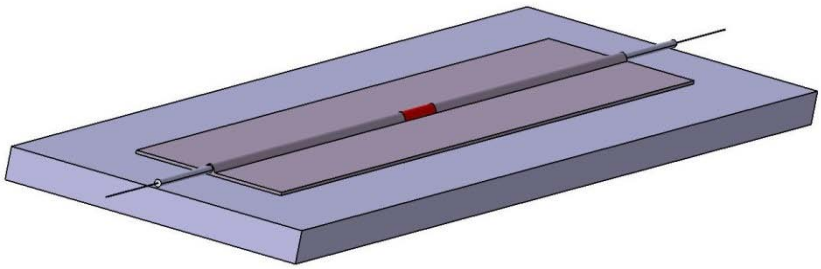

**Fig.1.** Schematic of the FORT concept attached to a coupon, the red area indicates the possible position of the FBG sensor

## 2. Basic principles of FBG sensors

Fiber Bragg grating sensors are actually spectral filters, which utilize the principle of Bragg reflection. The gratings are a series of parallel lines close together, inscribed in the core of an optical fibre. Optical fibres are exposed to a periodic pattern of ultraviolet light and, as a result, the gratings consist of alternating regions of high and low refractive indices. The

periodic grating acts as a filter, reflecting a narrow wavelength range, centered about a peak wavelength. This wavelength is known as the Bragg wavelength, $\lambda_B$, and is given by:

$$\lambda_B = 2n_{eff}\Lambda \qquad (1)$$

where $n_{eff}$ is the average refractive index and $\Lambda$ is the grating period. When a mechanical or thermal load is applied to the structure, the grating is strained and thus, there is a change of the peak reflected wavelength [1]. This way, the grating works as a strain sensor. Assuming that there is no change in the pressure, the change of the reflected wavelength is given by:

$$\frac{\Delta\lambda_B}{\lambda_B} = [1-(\frac{n_{eff}^{\ 2}}{2}(p_{12}-v(p_{11}+p_{12}))]\varepsilon + (a+\xi)\Delta T = F_G\varepsilon + (a+\xi)\Delta T \qquad (2)$$

where $\Delta\lambda_B$ is the wavelength shift, $\lambda_B$ is the initial reference wavelength, $v$ is the Poisson's ratio of the fibre, $p_{11}$ and $p_{12}$ are the elasto-optic coefficients of the elasto-optic tensor constants of the strain optic tensor and $F_G$ represents in total the gauge factor of the fibre. $\alpha$ is the coefficient of thermal expansion of the glass fibre, $\xi$ is the fibre thermo-optic coefficient, and $\Delta T$ is the temperature change. For typical germanosilicate fibres, the gauge factor $F_G$ equals to 0.773 and the wavelength–temperature sensitivity ($\alpha+\xi$) of a 1550 nm FBG is in the region of 10 pm $^{o}C^{-1}$.

## 3. Experimental procedure

### *3.1 Specimen manufacturing and sensorization*

Three point bending fatigue tests were scheduled in order to test the reliable long-term operation of the FORTs. The specimens were manufactured according to the ASTM D7264/D7264M-07 standard Test Method for Flexural Properties of Polymer Matrix Composite Materials. Carbon fiber reinforced plates with dimensions of 300x300 $mm^2$ were

manufactured in-house via the autoclave technique, at a stacking sequence $[+45/-45/0_2/90/0_2/90/0/90/0]_s$ using uni-directional M21/34%/UD194/IM7-12k carbon fabric prepreg by Hexcel. Two plates were fabricated with a final average thickness of 4.09mm.

Two groups of coupons were cut at dimensions 400x20 $mm^2$, the first group was sensorized with FORTs via co-bonding and the other via the secondary bonding approach.

The FORTs were manufactured by KVE Composites Group (Netherlands) via a simple autoclave process utilizing a specially designed mould. The optical fibre is protected from possible damage during the manufacturing by a low modulus teflon tubing, except the region of the FBG sensor.

Single-mode optical fibers with polyimide coating were utilized and put inside the FORTs, with one FBG sensor of central wavelength at 1540 nm. The optical fibre has a core diameter of 9 μm, cladding diameter of 125 μm, polyimide coating diameter up to 155 μm and the FBGs have a typical length of about 3-5 mm and were purchased by QPS Photronics Inc (Canada).

In the case of the co-bonding procedure, the FORT was placed on top of the uncured laminate (see Fig.2) and followed the same auto-clave curing cycle as the plate. In the case of the secondary bonding, the FORT was bonded on the surface with the appropriate adhesive (Hysol EA9394) after the completion of the curing cycle following a special process. Table 1 summarizes the two processes which can be utilized for the FORT sensorization of any composite structure.

**Table 1**

FORT mounting processes on a composite structure

| **Co-bonding process** | **Secondary bonding process** |
|---|---|
| 1. Laminate the carbon plies on the mold | 1. Mark the ribbon position using adhesive tape on |

2. Mark on the peel-ply the exact ribbons position
3. Hole the peel-ply for the passage of PTFE tubing
4. Position the ribbons inserting PTFE tubing in the peel-ply holes
5. Position the assembly (peel-ply + ribbons) on the laminate
6. Insert the two flexible caul-plates between peel-ply and FO (exiting from the holes) and apply a light pressure on the ribbons
7. Apply the perforating PTFE film, bleeder, PTFE film, rubber layer, vacuum bag
8. Apply the Cycom 977-2 curing cycle in autoclave

the laminate side where the FO exit

2. Cover the side of the laminate surface that doesn't process for surface preparation
3. Use wire netting to slightly roughing the surface
4. Use MEK to clean the laminate and the ribbon surface
5. Fix the laminate on the mold by using tacky tape
6. Position rubber layers on the laminate side with FO
7. Position the caul-plate between the laminate/rubber and the FO and fix it
8. Remove all the adhesive tape
9. Prepare the material for vacuum bag
10. Preset the oven temperature at 75 °C
11. Prepare the mixture of Hysol EA9394 (Part A 100, Part B 17)
12. Spread a flat layer of the mixture on the ribbons surface
13. Remove the excessive adhesive with spatula
14. Fix the ribbons on the laminate and the FO on the mask by using adhesive tape
15. Prepare the vacuum bag and apply the Hysol EA9394 curing cycle in oven

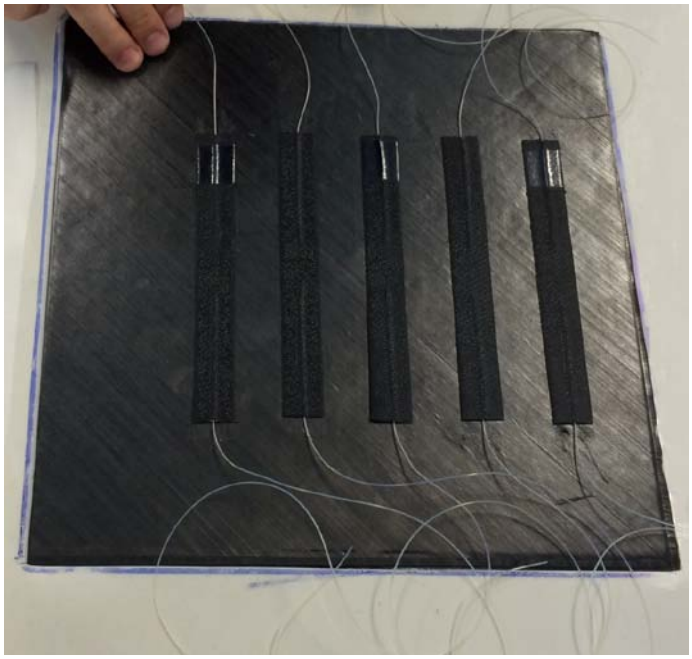

**Fig.2.** The composite plate in the FORT co-bonding case prior to the curing process

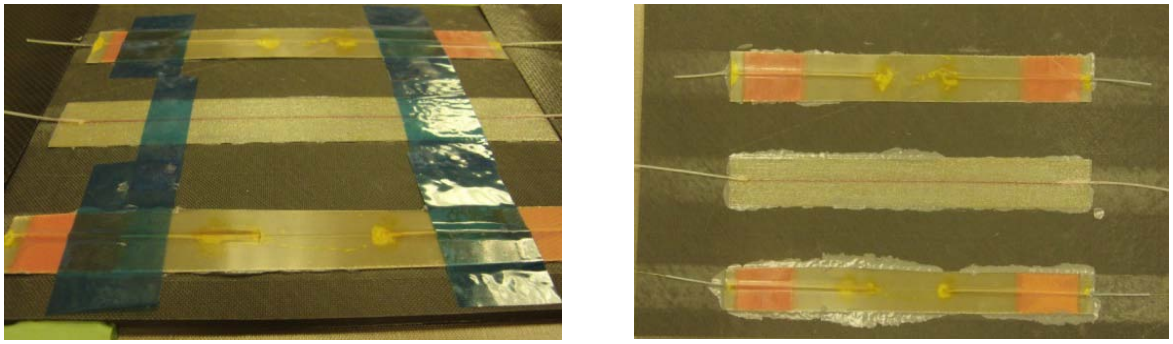

**Fig.3.** Example of the secondary bonding process

To mitigate the risk of optical fibre failure due to bending at the egress of the fiber from the FORT, special care was taken. A rubber layer surrounding the plate and an extra carbon fibre caul plate were used to ensure that the optical fibre will not fail or bend enough to jeopardize the proper light transmission (increasing too much the attenuation).

After having mounted the FORTs on the coupons, the next step was to attach electrical strain gauges (ESGs) to the specimens for comparison reasons and validation of the durability and proper function of the FBG sensor inside the FORT. The specimens were properly sanded and cleaned with acetone in the location where the ESG would be mounted for optimum adhesion.

The ESG was placed on the upper layer of the FORT exactly on top of the FBG. Model KFG-5-120-D16-11N30C2 of Kyowa was used. Two Kyowa DPM-611 B strain amplifiers were also used, as well as a National Instruments data acquisition board to record, digitize and transfer the ESG measurements to LabVIEW. The sensors topology on a representative coupon is depicted schematically in Fig.4. The distance of each sensor (FBG, ESG) from the specimen surface is measured and compensated for the correct and realistic interpretation of the measurement data. The loading nose has a special configuration (shown in Fig.5) so as not to exert load on the FORT in the area where the ESG is mounted.

The last step prior to test the coupons was to fusion splice the optical fiber with a pig-tail FC-APC connector in order to connect the FBG with a Micron Optics SM130 laser interrogator.

As mentioned above the excess optical fibre length should be carefully placed and secured on the structure to avoid damage on the optical fiber during the autoclave process. Although this step looks easy for the given geometry, it can become extremely demanding for complex geometries and structures. On the other hand the secondary bonded solution poses an ease of use. An issue of the procedure that can be improved is the amount and the uniformity of the adhesion layer. A system to provide a layer of uniform thickness and amount is under development. The use of adhesive in film form is also an interesting alternative. The greatest advantage of the secondary bonding approach is the ability to place FORTs anywhere upon the structure (even after manufacturing and assembly) offering thus the freedom and the versatility to design SHM tasks any time during the service life of the structure.

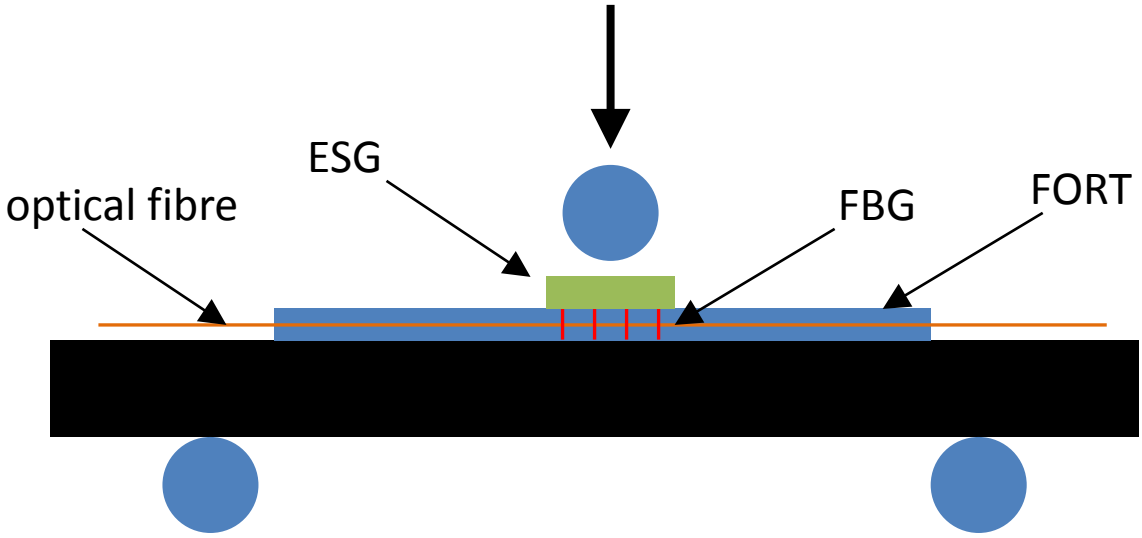


**Fig.4.** A schematic depiction of the positions of the FBG and the ESG

### *3.2 Test campaign*

To prove the feasibility of the FORTs to operate accurately and reliably as strain gauges, a series of tests was conducted. At first static tests were chosen to monitor the response of the FBGs and compare them to those of the electrical strain gauges in order to validate the working condition of the FBGs after the co-bonding or secondary bonding and fusion splicing. After this first validation testing, the procedure continued as planned, with the fatigue testing.

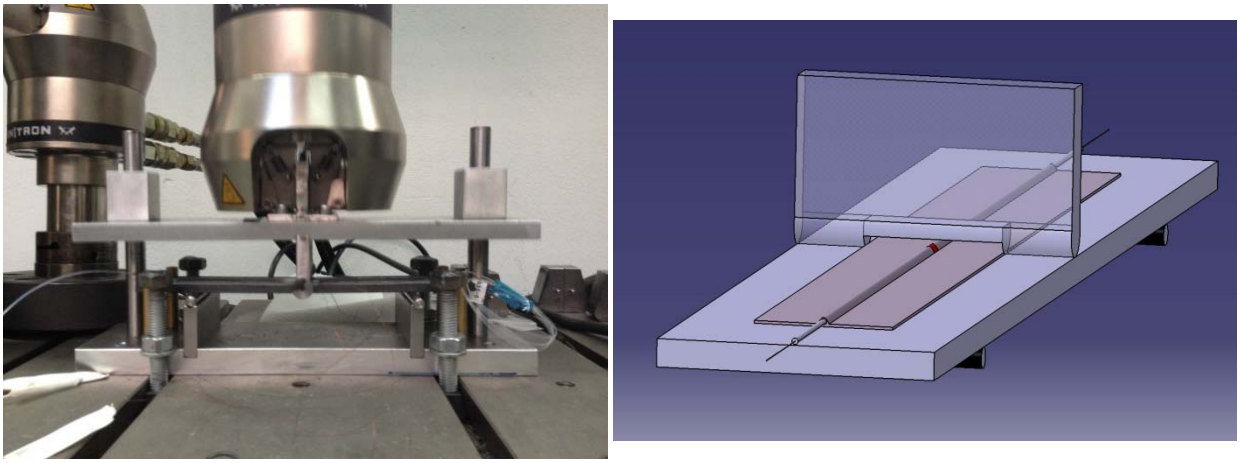

**Fig.5.** Three point bending test setup (actual and schematic)

Three point bending tests were performed on a fixture specially designed for the experimental purposes (Fig.5). It was fixed on an Instron servo-hydraulic 8872 universal testing machine and cyclic loading forces were imposed to the specimens. The fatigue ratio was set at R=0.1, the testing frequency at 10 Hz and the desired strain range was in the 400με-4000με region, significantly lower than the failure strain of this laminate at the regime of about 12000 με. Both the FBF and the ESG sensors were placed on the compressive surface of the test samples. To achieve the desired strains during testing the machine was set to apply a constant sinusoidal displacement, the amplitude of which was calibrated by analytical solutions as well as the indications of the gauges. The applied displacement led to a maximum load of approximately 1 kN. The fatigue test was repeated for 5 specimens of each FORT mounting case, (co-bonded and secondarily bonded). During every test, data of the machine displacement and the applied load were recorded. On each coupon, the axial strain in the middle of the upper surface of the specimen was recorded by one ESG and one FORT. Since the ESG was utilized for comparison reasons and validation of the FORT it was important to be located on the exact same spot on the coupon's surface. Obviously this is not exactly possible since the FBG sensor is embedded in the FORT. A direct comparison is not feasible since the two gauges were mounted in the same length and width but not in the same distance from the neutral axis of the coupon and thus the two measurements are not directly comparable, at least not without a correction. After testing, few specimens were cut in order to determine the exact distance of the FBG and the ESG from the coupon's neutral axis via optical microscopy (Fig. 6). The distance between the coupon surface and the FBG for the co-bonded specimens was measured at 0.266mm. In the case of the secondarily bonded specimens this distance is increased by 0.5 mm due to the extra adhesive layer. A height correction of the ESG value via Finite Element analysis is described in section 4 in order to render the two experimental values comparable. Based on analytical calculations we

confirmed that the bending stiffness of FORT is almost negligible compared with the bending stiffness of the tested coupons and thus it was assumed that the neutral axis of the specimen/FORT assembly remains unaffected. More details are found in section 6.

To further increase the accuracy of the results the exact position of the FBG along the optical fiber was verified. This was accomplished with the use of a soldering iron and the monitoring of the FBG wavelength shift. When the soldering iron passed over the FBG, the shift in temperature changed the wavelength. The exact position with accuracy of 1 mm led to an increase of ~8% to the accuracy of the calculated bending moment for the Finite Element Analysis (FEA) and the theoretical analysis (Section 4).

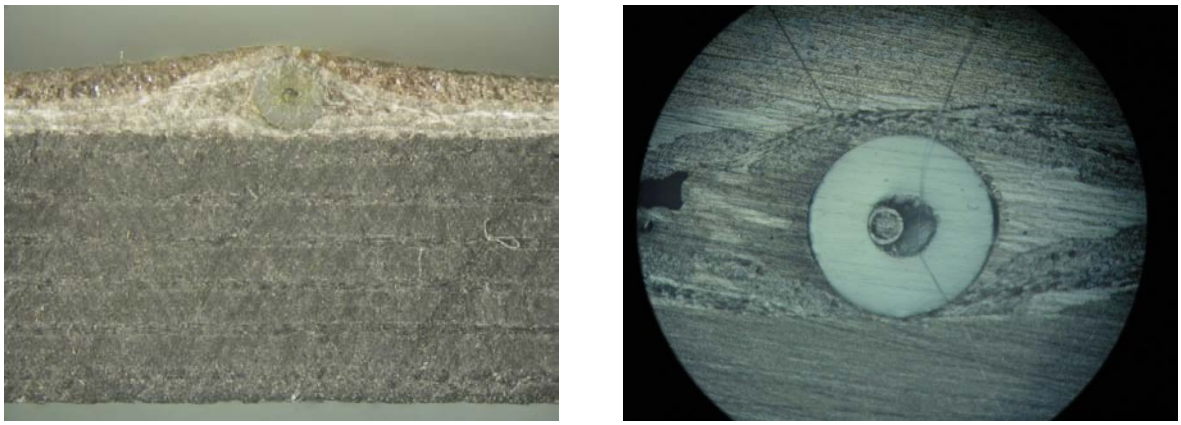

**Fig.6.** Cross Section of a co-bonded specimen a) macroscopic view b) under the optical microscope

### *3.3 Temperature variation during test*

During fatigue loading in polymer composite materials a temperature rise has been observed due to hysteretic heating and has been mainly attributed to internal damping [23] and to a lesser extent due to heat generation produced by damage mechanisms such as frictional sliding along fibre-fibre and fibre-matrix interfaces. Carbon fibre reinforced plastics are generally less prone to this phenomenon thanks to the high thermal conductivity of the carbon fibers. Additionally, the loading in our case is rather moderate at about 35% of the ultimate

bending load. Nevertheless, in order to define if the strains measured are influenced by a temperature increase or are of purely mechanical nature, the temperature rise was recorded via during a typical fatigue test. A thermocouple was placed on the surface of the FORT offering thus an indirect indication of the temperature field within the FORT, in the vicinity of the FBG sensor. As Fig.7 suggests, the temperature rises from the room temperature of ~23.5 $^{o}$C to about 25 $^{o}$C after a million cycles having already reached a plateau. Consequently, the effect of temperature variation can be safely considered negligible during the test.

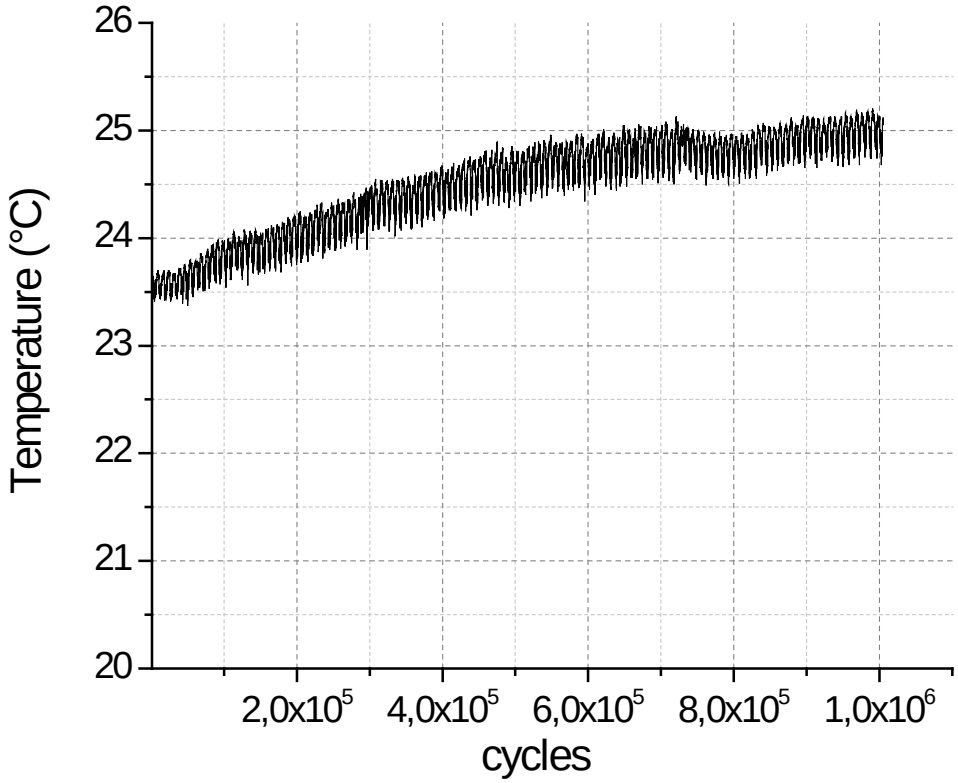


**Fig.7.** Temperature variation during a typical test measured by a thermocouple on the FORT's surface

## 4. Theoretical and numerical analysis

In order to verify the accuracy and the precision of the FORT measurements as well as to have knowledge of the anticipated strains to be developed during testing, the mechanical

response of the coupons was modeled both with FEA and analytically. Laminated composites are usually modeled using shell elements in MSC PATRAN. In the case of a relatively thick laminate as is the present one, solid elements can be also used. However, this option introduces certain disadvantages since solid elements tend to be overly stiff in bending. Thus, shell elements formulation was considered. Solid shell composite elements are also known as continuum shell composite elements. Hex8 8-node elements were chosen for the meshing as they are the most appropriate for the solid shell analysis.

In total 1000 elements and 1683 nodes were used, evenly distributed across the specimen. Material properties were taken into account according to Table 2. The specimen was modeled under realistic loads as recorded by the testing machine in specific cycles and the load was distributed across the top surface of the specimen except the area of the FBG as in reality. The solid shell analysis involves the use of shear correction factor in the calculation of the strains since the Kirchoff assumptions are no longer valid under large displacements and rotations in the 3-p bending configuration.

Simply supported boundary conditions are applied at the reference points of the rigid supports below the laminate representing the test fixture. Boundary conditions are applied at rigid surfaces instead of constraining the ply nodes as the local stresses due to the constraints edge effects disperse over greater distances of the structure because of the composite's anisotropy. The applied distributed load was introduced at the centre line except the region of the FORT sensor (so as not to damage it), exactly as the actual loading configuration stands (see Fig.5). Convergence checks were applied in order to conclude to the above given discretization. The final model is shown in Fig.8.

**Table 2**

Material properties for FE modeling

| Material | Thickness | Mechanical properties |
|---|---|---|
| Hexcel M21/T800S UD prepreg | 0.18 μm | $E_{11}$=164 GPa<br>$E_{22}$=8 GPa<br>$E_{33}$=8 GPa<br>$v_{12}$=$v_{21}$=0.3, $v_{31}$=0.0146<br>$G_{12}$=$G_{13}$=4.5 GPa<br>$G_{23}$=4.05 GPa |
| Woven glass prepreg (FORT) | 0.2 | $E_{11}$=30.3 GPa<br>$E_{22}$=27.6 GPa<br>$E_{33}$=27.6 GPa<br>$v_{12}$=$v_{21}$=0.123, $v_{31}$=0.112<br>$G_{12}$=$G_{13}$=4.41 GPa<br>$G_{23}$=4.05 GPa |
| Adhesive | 0.18 mm | E=4.237 MPa, v=0.3 |

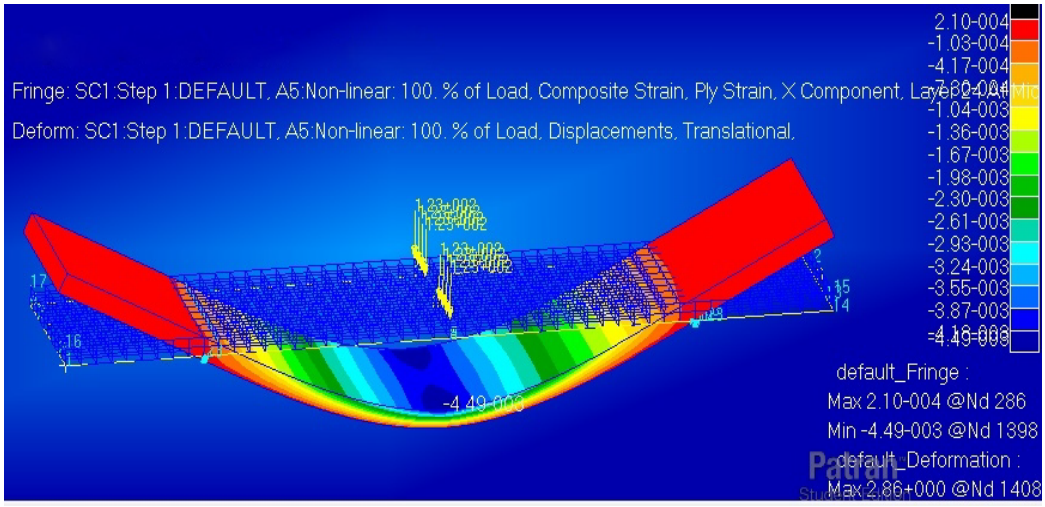


**Fig.8.** The developed FE model under loading

The numerical solution indicates a difference of 8.35% and 9.91%, for the co-bonded and secondarily bonded case respectively, between the FBG and ESG measurement due to the

height difference between them. This correction factor is taken into account in the results section.

Regarding the analytical approach, a first order shear deformation theory was utilized in order to include the contribution of transverse shear strains to the resulted strain since the assumption of small displacements/rotations (geometric linearity) is not valid in our tests. Details about the exact procedure and relevant equations can be found in Reddy [24].

## 5. Results

Upon the completion of the static and fatigue tests, a detailed analysis of the experimentally measured strain response was conducted and compared with strains obtained from analytical solution as well as FEA. Fig.9a and 9b show the results of strain measurements obtained by the FBG and ESG sensors under quasi-static loading for the co-bonded and secondarily bonded coupons respectively. In both cases there is a fair agreement between the two measurements with the maximum deviation reaching ~7%.

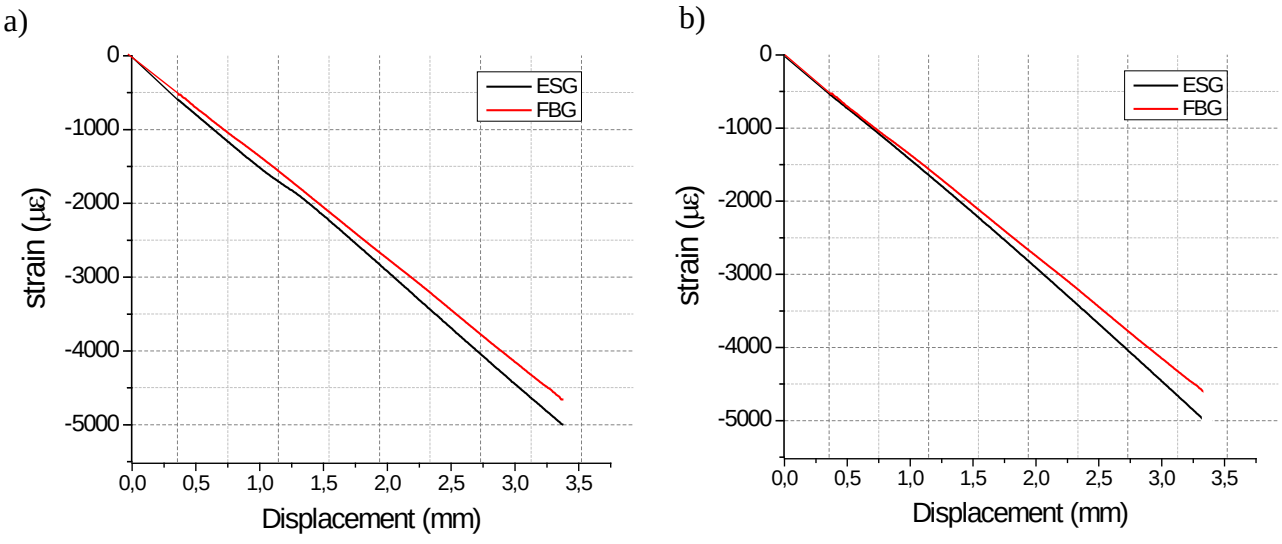


**Fig.9.** Quasi-static 3-point bending tests and comparison between FBG and ESG a) Secondarily bonded coupon b) co-bonded coupon

If the height difference correction of 8.35% and 9.91% that FE analysis in the previous section offered is taken into account then it is apparent that the deviation becomes minimal.

The data of the fatigue tests are presented in the form of graphs, of strain cycles during specific loading cycles.

Fig.10 depicts the strain measurements of the FBG and the ESG on a co-bonded coupon during the entire fatigue test. ESG values in Fig.10 are not corrected for height difference and this explains why they are about 10% higher compared to the FBG readings. The superiority of the FBG readings and of the FORT operation in total is manifested via their stability and repeatability. The ESG on the contrary works properly up to ~640 kcycles when its values begin to deviate. Probably the adhesion of the ESG to the surface of the FORT where it is mounted is compromised. The ESGs tended to de-bond from the coupon surface after approximately 600.000 cycles. This happened for 8 out of 10 tested coupons with a random pattern on the ESG "failure" cycle.

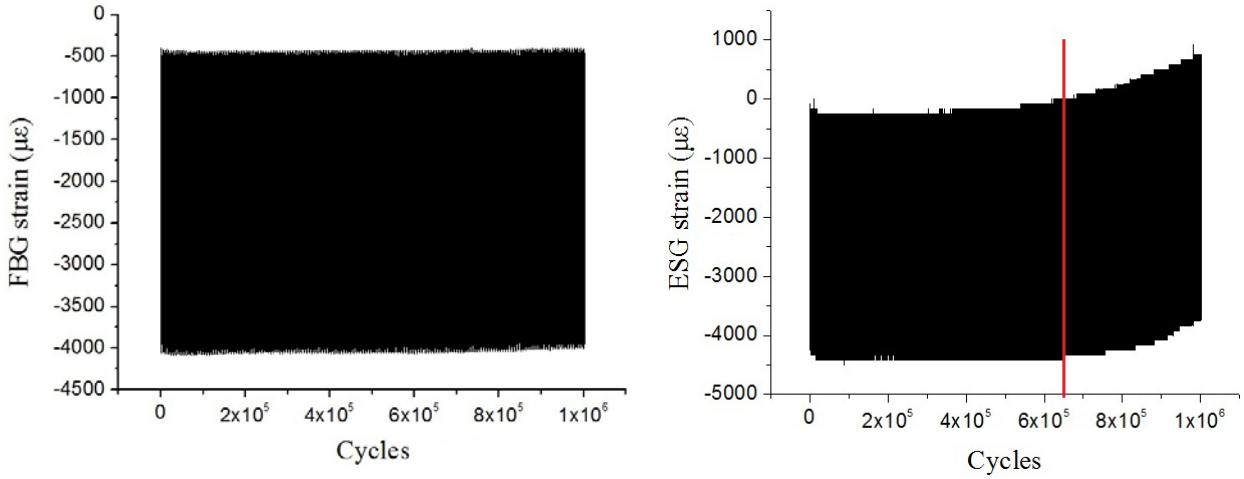


**Fig.10.** Strain measurements during fatigue loading for the FBG and the ESG gauges

In Fig.11 and Fig.13 comprehensive graphs of the progress of the strain monitoring during fatigue test for the secondary bonded and the co-bonded FORT mounting technique are

presented respectively. Cycles $10^3$, $10^4$, $10^5$, $5{\cdot}10^5$, $10^6$ were selected as a representative sample, analyzed and presented. The evolution of the experimental (FBG and corrected ESG) as well as the theoretically and numerically calculated strain values is depicted. In order to assess how the FBG value is compared to ESG, theoretical and FEA values, the Root-Mean Square Deviation (RMSD) for the selected cycles is calculated and presented in Tables 3 and 4. For the calculation of the RMSD value Eq. 3 was utilized.

$$RMSD = \frac{\sqrt{\Sigma(x_i - y_i)^2}}{\Sigma y_i^2} \qquad (3)$$

As shown in Table 3, the root mean square deviation between the FBG strain measurement and strain either measured using ESG or calculated remains well below 7%. The large deviation of 15% between FBG and ESG after $10^6$ cycles is due to the ESG detachment from the coupon surface (see Fig.10b).

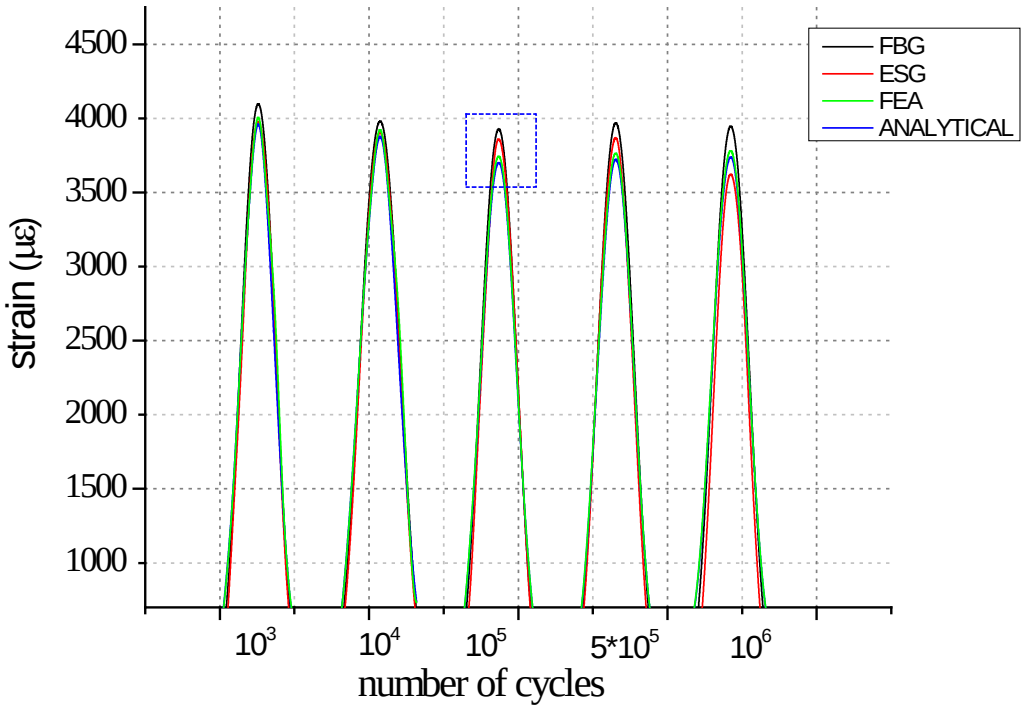


**Fig.11.** The secondarily bonded coupon's strain response as recorded by all sensors and calculated analytically and with FEA (please refer to the online version for a colored version of the figure)

**Table 3**

RMSD between FBG and other values for all the cycles of secondarily bonded coupons

| **FBG vs ESG** | | **FBG vs analytical** | | **FBG vs FEA** | |
|---|---|---|---|---|---|
| Cycle | RMSD % | Cycle | RMSD % | Cycle | RMSD % |
| $10^3$ | 4,98 | $10^3$ | 5,99 | $10^3$ | 4,82 |
| $10^4$ | 3,39 | $10^4$ | 5,13 | $10^4$ | 3,59 |
| $10^5$ | 5,35 | $10^5$ | 6,21 | $10^5$ | 5,41 |
| $5{\cdot}10^4$ | 5,74 | $5{\cdot}10^4$ | 6,36 | $5{\cdot}10^4$ | 5,44 |
| $10^6$ | 15,13 | $10^6$ | 6,62 | $10^6$ | 6,24 |

Zooming at the top of strain graphs during the $10^5$ cycle (Fig.12) provides a clearer local view of the various measurements and numerical/analytical calculations. The deviation of the FBG value to the ESG (corrected value to compensate for the height difference between the two gauges) is a mere 2%, with the FE as well as the analytical value deviating up to ~6%, obviously due to the assumptions made in each case.

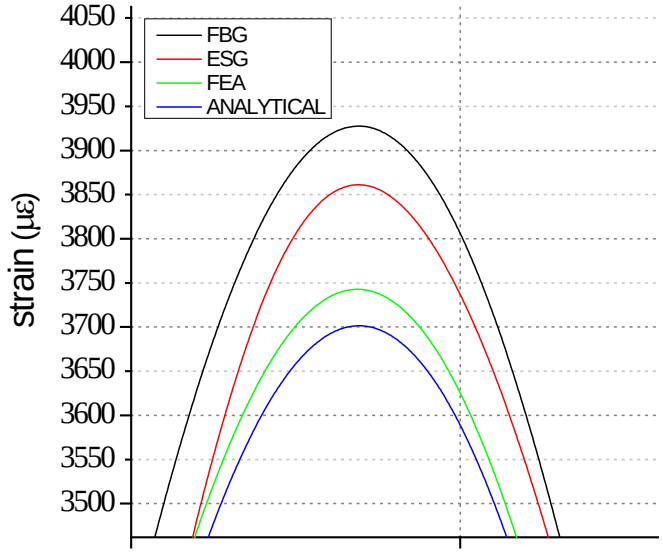


**Fig.12.** A zoom in the top of the $10^5$ cycle of a secondarily bonded specimen (please refer to the online version for a colored version of the figure)

Similar behavior was observed for the co-bonded FORTs as demonstrated in Fig.13. The problem of the ESG de-bonding is observed on the co-bonded coupons as well. In Table 4, the low RMSD values prove the reliable FORT operation in contrast to ESGs which seem to 'fail' after a certain operational period.

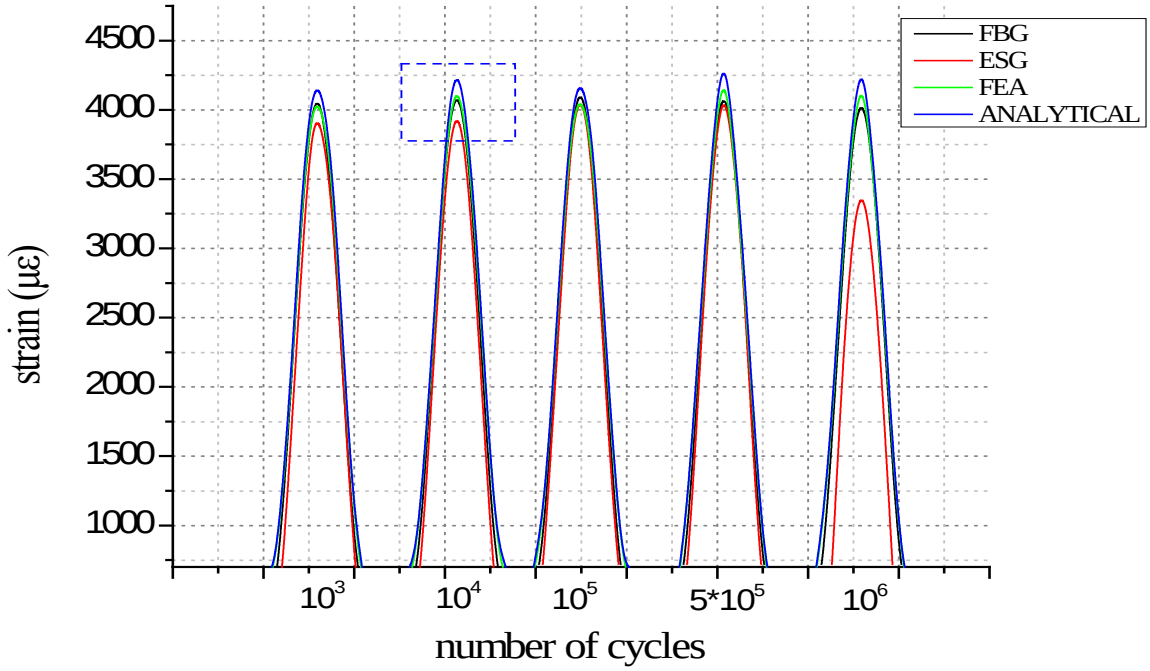


**Fig.13.** The co-bonded coupon's strain response as recorded by all sensors and calculated analytically and with FEA (please refer to the online version for a colored version of the figure)

**Table 4**

RMSD between FBG and other values for all the cycles of co-bonded coupons

| **FBG vs ESG** | | **FBG vs analytical** | | **FBG vs FEA** | |
|---|---|---|---|---|---|
| Cycle | RMSD (%) | Cycle | RMSD % | Cycle | RMSD % |
| $10^3$ | 5,02 | $10^3$ | 5,84 | $10^3$ | 4,78 |
| $10^4$ | 3,32 | $10^4$ | 5,45 | $10^4$ | 3,45 |
| $10^5$ | 5,39 | $10^5$ | 6,12 | $10^5$ | 5,12 |

| | | | | | |
|---|---|---|---|---|---|
| $5 \cdot 10^4$ | 5,48 | $5 \cdot 10^4$ | 6,03 | $5 \cdot 10^4$ | 5,31 |
| $10^6$ | 19,75 | $10^6$ | 6,54 | $10^6$ | 6,17 |

Exemplary, a zoom in the top of the $10^4$ cycle gives in Fig.14 a clearer local view of the various measurements and numerical/analytical calculations. The deviation of the FBG value to the ESG (corrected value to compensate for the height difference between the two gauges) is about 4% with the analytical value deviating up to another 4%.

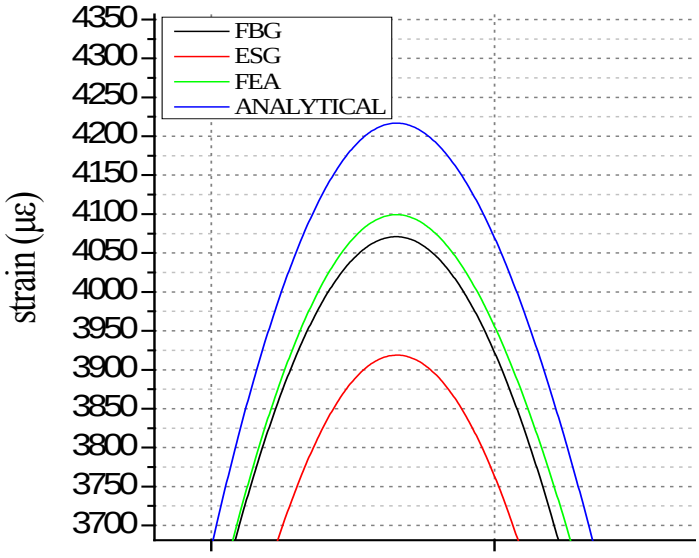


**Fig.14.** A zoom in the top of the $10^4$ cycle of a co-bonded specimen (please refer to the online version for a colored version of the figure)

## 6. Effect of FORT on the dynamic characteristics of a composite subcomponent

In order to use the FORT on large scale structures and especially in the case of many FORTs being used simultaneously, a study of the effect of the FORT presence on the dynamic characteristics of a typical aeronautic structure is conducted. The structure selected is a 1m long C-section CFRP beam representative of a front spar of a wing. Fig.15 shows the

structural details and the position of the eight FORTs used to sensorize the beam. The section dimensions are 100x100 $mm^2$ with a thickness of 3.2 mm. It was discretized utilizing 1380 shell elements and 2294 nodes.

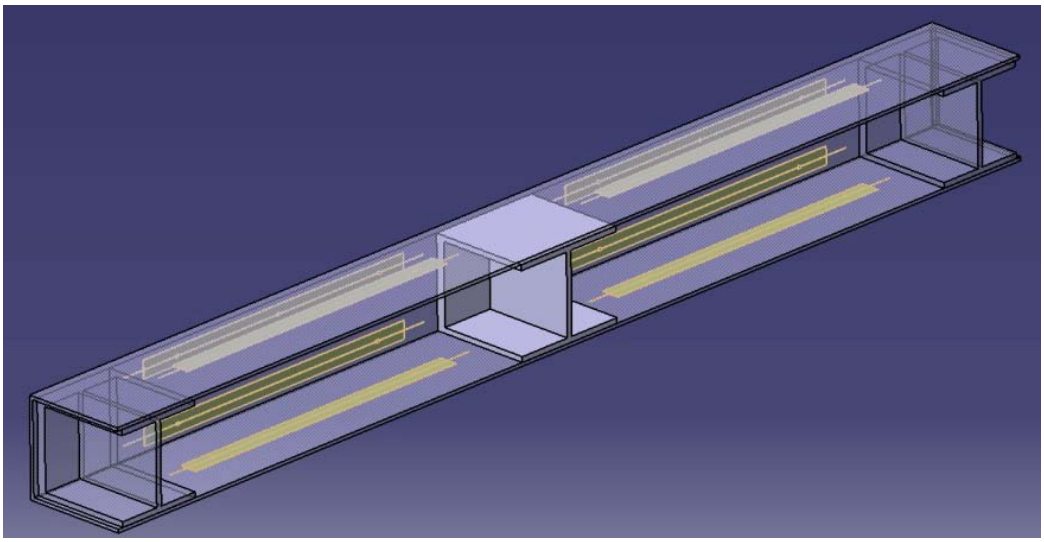

**Fig.15.** C-section CFRP beam sensorized with eight FORTs

To quantify the effect of FORTs on the structure's dynamic characteristics, FE models with and without FORTs were developed in MSC Patran utilizing the same material properties of Table 2. Modal analysis resulted in the eigen-frequencies and mode shapes of the respective models. The eigen-frequency comparison is rather straight-forward and the obtained results regarding the first ten eigen-values are summarized in Table 5. It is evident that the FORTs do not alter significantly the stiffness of the structure and consequently the maximum difference is of the order of 1,3%. In order to compare the eigen-modes of the models the Modal Assurance Criterion (MAC) is utilized. The MAC is a quantifiable correlation between the mode shapes and the values range from 0 (no correlation between shapes) to 100 (full correlation). The MAC between two vectors $\Phi_\alpha$, $\Phi_b$ is given by Eq.4:

$$MAC(\Phi_a, \Phi_b) = \frac{\left|\{\Phi_a\}^T\{\Phi_b\}\right|^2}{(\{\Phi_b\}^T\{\Phi_b\})\,(\{\Phi_a\}^T\{\Phi_a\})} \qquad (4)$$

Table 6 gives the MAC values for the first five numerically calculated modeshapes of the composite subcomponent with and without FORTs. The conclusion that the effect of FORTs

is minimal upon the mode shapes as well can be deduced by the fact that the diagonal MAC values are actually 1, which proves that they remain absolutely correlated even after the mounting of FORTs.

**Table 5**

Numerical eigen-frequencies comparison of the composite subcomponent with and without FORTs

| Eigen-frequency # | Model without FORTs (Hz) | Model with FORTs (Hz) | Δf (Hz) | Percentage difference (%) |
|---|---|---|---|---|
| 1 | 63,45 | 63,19 | -0,26 | 0,42 |
| 2 | 166,24 | 168,47 | 2,23 | 1,32 |
| 3 | 177,69 | 179,42 | 1,73 | 0,96 |
| 4 | 209,45 | 209,35 | -0,10 | 0,05 |
| 5 | 209,82 | 210,53 | 0,71 | 0,34 |
| 6 | 258,91 | 259,77 | 0,86 | 0,33 |
| 7 | 291,20 | 290,98 | -0,22 | 0,08 |
| 8 | 321,11 | 321,50 | 0,39 | 0,12 |
| 9 | 352,30 | 351,72 | -0,58 | 0,16 |
| 10 | 372,57 | 373,78 | 1,21 | 0,32 |

**Table 6**

MAC values for the comparison of the first five numerical modeshapes of the composite subcomponent with and without FORTs

Model without FORT

| Model with FORT | | | | | | |
|---|---|---|---|---|---|---|
| **MAC** | Mode 1 | Mode 2 | Mode 3 | Mode 4 | Mode 5 |
| Mode 1 | 1,00 | 0,63 | 0,76 | 0,59 | 0,51 |
| Mode 2 | 0,63 | 0,999 | 0,82 | 0,79 | 0,81 |
| Mode 3 | 0,76 | 0,81 | 0,999 | 0,61 | 0,60 |
| Mode 4 | 0,59 | 0,78 | 0,61 | 1 | 0,97 |
| Mode 5 | 0,50 | 0,81 | 0,60 | 0,97 | 0,999 |

## 7. Conclusions

In this study, the potential and the metrological reliability of FORTs for strain sensing of composite structures is evaluated versus classical electrical strain gauges. Two concept of mounting the sensors have been discussed, co-bonding during the autoclave process and secondary bonding using adhesive. Through extensive fatigue testing it is shown that FORTs can be reliably used as they provide accurate strain measurements over an extended operating spectrum of $10^6$ duty cycles. In addition the FORT measurements are more consistent as compared to the ESGs that detach from the surface of the structure after a certain number of cycles. Furthermore, FORTs offer all the advantages of FBG sensors plus they are readily replaceable in case of sensor failure or for maintenance issues. The obtained FORT strain measurements are in logical agreement with ESGs and with numerically and theoretically calculated strain values at the same locations. It is expedient to comment at this point on the issue of comparison of strain measurements or strain calculations. It is a common ground in many previous studies to consider ESG readings or FEA calculations as the baseline with

whom the FBG readings must agree. Actually this is a misconception since there is no absolute knowledge of the true strain on a certain spot upon a structure. Any experimental method has sources of error and any theoretical or numerical approach a series of assumptions. The deviations reported in this or past studies can be attributed to a number of reasons. For example, besides the different accuracy and precision between an FBG metrological configuration and an ESG one, these measurements are very sensitive to the relative misalignment between the sensors. The theoretical solution (even a higher order shear deformation theory) does not take into account boundary effects or the actual geometry whereas numerical calculations via FEA are approximate solutions that do not take into account the inhomogeneities (e.g. voids, ply thickness variations etc) or the inaccuracies in the pre-set mechanical properties of the plies. Obviously, the uncertainty on the exact ply mechanical properties affects also theoretical solutions. Consequently, the comparison between experimental strains and or numeric or theoretical ones is a relative task and one has to be very careful with any conclusions. Undeniably, FBG sensors embedded in FORTs can consistently and reliably perform their gauging task even in a high cycle high strain regime of as much as 4000 με, where ESG sensors have undoubtedly failed.

Finally, it was demonstrated that the effect of FORTs on a sensorized representative composite subcomponent regarding the dynamical properties of the structure is minimal both on eigen-frequencies and mode shapes, rendering the FORT concept an attractive, reliable solution for strain sensing of composite structures.

## 8. Acknowledgements

The major part of the present work has been funded within the frame of FP7 SARISTU project (grant agreement No 284562). The FORTs in the present work were developed and manufactured by our SARISTU partner KVE Composites Group and the authors kindly acknowledge their contribution.

## References

1. Boller C and Staszewski WJ, Aircraft Structural Health and Usage Monitoring. In: Staszewski W J, C Boller and G R Tomlinson, editors. Health Monitoring of Aerospace Structures, John Wiley & Sons, 2003, p. 29-73.
2. Boller C, Chang F-K and Fujino Y, Encyclopedia of Structural Health Monitoring. John Wiley & Sons, 2009
3. Loutas TH, Panopoulou A, Roulias D, Kostopoulos V. Intelligent health monitoring of aerospace composite structures based on dynamic strain measurements. Expert Systems with Applications 2012; 39 (9): 8412-8422,
4. Panopoulou A, Loutas T, Roulias D, Fransen S, Kostopoulos V. Dynamic fiber Bragg gratings based health monitoring system of composite aerospace structures. Acta Astronautica 2011;69 (7-8): 445-457,
5. Takeda S, Aoki Y, Ishikawa KK, Takeda N, Kikukawa H. Structural health monitoring of composite wing structure during durability test. Composite Structures 2007;79:133–9
6. Connolly, C. Fibre-optic-based sensors bring new capabilities to structural monitoring. Sensors Review 2006; 26: 236-243
7. Todd MD, Nichols JM, Trickey ST, Seaver M, Nichols CJ, Virgin LN. Bragg grating-based fibre optic sensors in structural health monitoring. Philosophical Transactions of the Royal Society A: Mathematical, Physical and Engineering Sciences 2007; 365 (1851): 317-343.

8. Measures RM. Smart composite structures with embedded sensors. Composites Engineering 1992;2(5–7):597–618.
9. Botsis J, Humbert L, Colpo F, Giaccari P. Embedded fiber Bragg grating sensor for internal strain measurements in polymeric materials. Optics and Lasers in Engineering 2005;43:491–510.
10. Minakuchi S, Umehara T, Takagaki K, Ito Y, Takeda N. Life cycle monitoring and advanced quality assurance of L-shaped composite corner part using embedded fiber-optic sensor. Composites: Part A Applied Science and Manufacturing 2013; 48: 153-161.
11. Papantoniou A, Rigas G, Alexopoulos N. Assessment of the strain monitoring reliability of fiber Bragg grating sensor (FBGs) in advanced composite structures. Composite Structures 2011; 93 (9): 2163-2172.
12. Wei CY, James SW, Ye CC, Dykes ND, Tatam RP and Irving PE. Strain capability of optical fibre Bragg grating sensing in composite smart structures. In: Proceedings of the 12th International Conference on Composite Materials, Paris, 1999, paper 443.
13. Levin K, Skontorp A. Fibre optic sensors in composite structures, In: Proceedings of the European Workshop on SHM, Paris, 2002: 530–537.
14. Hadzic R, John S and Herszberg I. Structural integrity analysis of embedded optical fibres in composite structure. Composite Structures 1999; 47 759–765.
15. Jensen DW, Pascal J and August JA. Performance of graphite/bismaleimide laminates with embedded optical fibers. Part I: Uniaxial tension. Smart Structures and Materials 1992; 1: 24–30.
16. De Baere I, Luyckx G, Voet E, Van Paepegem W, Degrieck J. On the feasibility of optical fibre sensors for strain monitoring in thermoplastic composites under fatigue loading conditions. Optics and Lasers in Engineering 2009; 47 (3-4): 403-411.

17. De Waele W, Degrieck J, Moerman W, Taerwe L, De Baets P. Feasibility of integrated optical fibre sensors for condition monitoring of composite structures Part I: Comparison of Bragg-sensors and strain gauges. Insight: Non Destructive Testing and Condition Monitoring 2003; 45 (4): 266-271
18. Groves RM, Chehura E, Li W, Staines SE, James SW and Tatam RP. Surface strain measurement: a comparison of speckle shearing interferometry and optical fibre Bragg gratings with resistance foil strain gauges. Measurement Science and Technology 2007; 18: 1175–1184
19. Friebele EJ, Askins CG, Putnam MA, Florio Jr J, Fosha Jr AA, Donti RP and Blosser PG, Distributed strain sensing with fiber Bragg grating arrays embedded in CRTM™ composites. Electronics Letters 1994; 30: 1783–1784.
20. Friebele EJ, Askins CG, Putnam MA, Heider PE, Blosser RG, Florio Jr J, Donti RP, and Garcia J, Demonstration of distributed strain sensing in production scale instrumented structures, In: Proceedings of SPIE - The International Society for Optical Engineering 1996; 2721: 118-124.
21. Kalamkarov AL, MacDonald DO, Fitzgerald SB, and Georgiades AV, Reliability assessment of pultruded FRP reinforcements with embedded fiber optic sensors, Composite Structures 2000; 50: 69–78.
22. Mrad N, Sparling S, and Laliberte J. Strain monitoring and fatigue life of Bragg grating fiber optic sensors, In: Proceedings of SPIE - The International Society for Optical Engineering 1999; 3670: 82–91.
23. Hetrzsberg R W and Manson. J A Fatigue of Engineering Plastics, New York: Academic, 1980.
24. J. N. Reddy, Mechanics of Laminated Composite Plates and Shells: Theory and Analysis, Second Edition, CRC Press, 2003.